

Overdensities of SMGs around *WISE*-selected, ultraluminous, high-redshift AGNs

Suzy F. Jones,¹★ Andrew W. Blain,² Roberto J. Assef,³ Peter Eisenhardt,⁴ Carol Lonsdale,⁵ James Condon,⁵ Duncan Farrah,⁶ Chao-Wei Tsai,^{4,7} Carrie Bridge,⁴ Jingwen Wu,⁸ Edward L. Wright⁷ and Tom Jarrett⁹

¹Department of Space, Earth, and Environment, Chalmers University of Technology, Onsala Space Observatory, SE-43992, Onsala, Sweden

²XROA, Department of Physics and Astronomy, University of Leicester, University Road, Leicester LE1 7RH, UK

³Núcleo de Astronomía de la Facultad de Ingeniería, Universidad Diego Portales, Av. Ejército Libertador 441, Santiago, Chile

⁴Jet Propulsion Laboratory, California Institute of Technology, 4800 Oak Grove Dr, Pasadena, CA 91109, USA

⁵National Radio Astronomy Observatory, 520 Edgemont Road, Charlottesville, VA 22903-2475, USA

⁶Department of Physics, Virginia Polytechnic Institute and State University, MC 0435, 850 West Campus Drive, Blacksburg, VA 24061, USA

⁷Department of Physics and Astronomy, University of California, Los Angeles, 430 Portola Plaza, Los Angeles, CA 90095-1547, USA

⁸National Astronomical Observatories, Chinese Academy of Sciences, 20A Datun Road, Chaoyang District, Beijing 100012, China

⁹Astronomy Department, University of Cape Town, Rondebosch 7701, Republic of South Africa

Accepted 2017 May 9. Received 2017 May 4; in original form 2016 August 4

ABSTRACT

We investigate extremely luminous dusty galaxies in the environments around *Wide-field Infrared Survey Explorer* (*WISE*)-selected hot dust-obscured galaxies (Hot DOGs) and *WISE*/radio-selected active galactic nuclei (AGNs) at average redshifts of $z = 2.7$ and 1.7 , respectively. Previous observations have detected overdensities of companion submillimetre-selected sources around 10 Hot DOGs and 30 *WISE*/radio AGNs, with overdensities of ~ 2 – 3 and ~ 5 – 6 , respectively. We find that the space densities in both samples to be overdense compared to normal star-forming galaxies and submillimetre galaxies (SMGs) in the Submillimetre Common-User Bolometer Array 2 (SCUBA-2) Cosmology Legacy Survey (S2CLS). Both samples of companion sources have consistent mid-infrared (mid-IR) colours and mid-IR to submm ratios as SMGs. The brighter population around *WISE*/radio AGNs could be responsible for the higher overdensity reported. We also find that the star formation rate densities are higher than the field, but consistent with clusters of dusty galaxies. *WISE*-selected AGNs appear to be good signposts for protoclusters at high redshift on arcmin scales. The results reported here provide an upper limit to the strength of angular clustering using the two-point correlation function. Monte Carlo simulations show no angular correlation, which could indicate protoclusters on scales larger than the SCUBA-2 1.5-arcmin scale maps.

Key words: galaxies: active – galaxies: clusters: general – galaxies: high-redshift – quasars: general – infrared: galaxies – submillimetre: galaxies.

1 INTRODUCTION

Advances in infrared (IR) telescope technology like the NASA’s *Wide-Field Infrared Survey Explorer* (*WISE*; Wright et al. 2010) have enabled observations of luminous active galactic nucleus (AGN) that have been difficult to find with previous IR missions. *WISE* is able to find luminous, dusty, high-redshift, active galaxies because the hot dust heated by AGN and/or starburst activity can be traced using the *WISE* 12- μm (*W3*) and 22- μm (*W4*) bands. Eisen-

hardt et al. (2012), Bridge et al. (2013) and Lonsdale et al. (2015) have shown that *WISE* can find different classes of interesting, luminous, high-redshift, dust-obscured AGNs.

Eisenhardt et al. (2012) and Wu et al. (2012) observed galaxies with faint or undetectable flux densities in the 3.4- μm (*W1*) and 4.6- μm (*W2*) bands, and well-detected fluxes in the *W3* and/or *W4* bands, with a radio blind selection, giving a ‘*W1W2*-dropout’ selection yielding hot dust-obscured galaxies (Hot DOGs).

Another population of luminous, dusty, *WISE*-selected AGNs were found by Lonsdale et al. (2015), by combining *WISE* and National Radio Astronomy Observatory (NRAO) Very Large Array (VLA) Sky Survey (NVSS; Condon et al. 1998) and/or Faint Images

* E-mail: suzy.jones@chalmers.se

of the Radio Sky at Twenty-cm (FIRST; Becker, White & Helfand 1995). They were selected in a similar method in the mid-infrared (mid-IR), and are a similarly high luminosity, dust-obscured population, and in this paper are known as *WISE*/radio AGNs. The strong compact radio emission could be from AGN jets (Lonsdale et al. 2015).

A sample of 10 Hot DOGs and 30 *WISE*/radio AGNs was observed with James Clerk Maxwell Telescope (JCMT) Submillimetre Common-User Bolometer Array 2 (SCUBA-2), and the fields around them were found to have an overdensity of submillimetre galaxies (SMGs)¹ by a factor of ~ 2.4 and ~ 5.6 , respectively, when compared with blank-field submm surveys in Jones et al. (2014, 2015). The Hot DOGs appeared to have redder mid-IR colours and less submm emission than *WISE*/radio AGNs, which could be due to selection effects (Jones et al. 2014, 2015). They have very similar spectral energy distributions (SEDs) and are both redder than standard AGN templates (see fig. 5 in both Jones et al. 2014 and 2015). The typical redshift of the 10 observed Hot DOGs is $z = 2.7$ (Jones et al. 2014), higher than the typical redshift of *WISE*/radio AGNs, $z = 1.3$ (Jones et al. 2015). Although only 10 out of the 30 *WISE*/radio AGN redshifts are spectroscopically known from the SCUBA-2 subset, from Lonsdale et al. (2015) redshifts for 45 out of 49 *WISE*/radio AGNs are known, and the typical value was $z = 1.7$.

Follow-up *Spitzer* Infrared Array Camera (IRAC) imaging of a subset of Hot DOGs found an overdensity of galaxies within 1 arcmin above the number observed in random pointings (Assef et al. 2015). They also found that Hot DOG environments are as dense as the clusters found by the Clusters Around Radio-Loud AGN surveys (Wylezalek et al. 2013, 2014).

Studying the environments of Hot DOGs and *WISE*/radio AGNs will help to understand the evolution of galaxies and the link with their host galaxy. This paper will explore the clustering and surface number density of the fields to study the environments surrounding the *WISE*-selected AGNs. Also the properties of the companion sources around Hot DOGs and *WISE*/radio AGNs will be investigated to determine their nature.

In Section 2, the surface number density and space density of SMG sources in the fields around Hot DOGs and *WISE*/radio AGNs are compared. In Section 3, the angular two-point correlation function is used to characterize the clustering of the companion SMGs around the *WISE*/radio AGNs. In Section 4, the properties of the companion sources in the Hot DOG and *WISE*/radio AGN fields are compared using submm, SFR estimations, star formation rate density (SFRD) estimates, mid-IR and radio data with previous surveys of companion SMG sources in the Hot DOG and *WISE*/radio-selected AGN fields. The nature and properties of the companion sources around Hot DOGs and *WISE*/radio AGNs are described in Section 5.

Throughout this paper, we assume a Λ cold dark matter cosmology with $H_0 = 71 \text{ km s}^{-1} \text{ Mpc}^{-1}$, $\Omega_m = 0.27$ and $\Omega_\Lambda = 0.73$. *WISE* catalogue magnitudes are converted to flux densities using zero-point values on the Vega system of 306.7, 170.7, 29.04 and

8.284 Jy for *WISE* 3.4, 4.6, 12 and 22 μm wavelengths, respectively (Wright et al. 2010).

2 COMPANION SOURCE DENSITY

JCMT SCUBA-2 observations of Hot DOGs and *WISE*/radio AGNs were in the ‘CV DAISY’ mode that produces a uniformly deep coverage 3-arcmin diameter map (Holland et al. 2013). 17 companion sources were detected at 3σ significance or above in 10 JCMT SCUBA-2 fields of Hot DOGs reported by Jones et al. (2014) with an average root mean square (rms) noise of $1.8 \text{ mJy beam}^{-1}$, as shown in Table 1.

81 companion sources were detected at 3σ or greater significance in 30 *WISE*/radio-selected AGN fields reported by Jones et al. (2015) with average rms noise of $2.1 \text{ mJy beam}^{-1}$, see Tables 2–5. They concluded that they have a higher density of SMGs when compared with Hot DOGs by an additional factor of 2.4 ± 0.9 (Jones et al. 2015). The *WISE*/radio AGNs have a lower redshift range, fewer of the *WISE*-selected AGNs are submm detected and lower total IR luminosities compared with Hot DOGs (Jones et al. 2014, 2015). The lower redshift range and higher overdensity of SMGs around *WISE*/radio AGNs can be seen in Fig. 1. While the observed Hot DOGs have a typically higher redshift than the *WISE*/radio AGNs, the companion sources are matched in submm luminosity (see Tables 1–5) and they are consistent with having similar mid-IR to submm ratios. The *K*-correction at wavelengths longer than 500 μm remains approximately constant with increasing redshift. Due to this *K*-correction effect, the SCUBA-2 fraction of SMG detection should be independent of redshift.

The detection level was set at 3σ or greater in order to have completeness but reduce the chance of spurious false-positive detections. However, there is controversy over whether 3σ is reliable (e.g. Coppin et al. 2005; Casey et al. 2012). Fig. 2 presents the signal-to-noise ratio (SNR) of the companion sources around Hot DOGs and *WISE*/radio AGNs and for the two data sets combined. As expected, the higher the SNR the fewer the sources detected and the less complete the sample. Jones et al. (2015) looked at the number of SMGs in the *WISE*/radio AGN fields detected at greater than 3σ and 4σ and compared to the LABOCA ECDFS Submm Survey (LESS; Weiß et al. 2009), and concluded that the overdensity of SMGs detected above 3σ is consistent with SMGs detected above 4σ .

Comparing these number counts to ‘blank-field submm’ surveys shows them to be overdense. The blank-field submm surveys used to compare were the LESS, Cosmological Evolution Survey (COSMOS; Casey et al. 2013) and the SCUBA Half-Degree Extragalactic Survey (SHADES; Coppin et al. 2006) fields. The Hot DOG fields have an SMG overdensity by a factor of ~ 2 – 3 compared with previous blank-field submm surveys, and the *WISE*/radio-selected AGN fields have an even greater overdensity, by a factor of ~ 5 – 6 (Jones et al. 2015). However, LESS fields could be underdense by a factor of ~ 2 e.g. Swinbank et al. (2014), and the overdensity factor of the Hot DOG fields is less secure, but compared to COSMOS and SHADES there is still an overdensity factor between 2 and 3.

The surface number density of SMGs in the Hot DOG fields is $866 \pm 210 \text{ deg}^{-2}$, and $1375 \pm 152 \text{ deg}^{-2}$ in the *WISE*/radio AGN fields, to a depth of 1.8 and $2.1 \text{ mJy beam}^{-1}$ (submm single dish), respectively. These are higher than previous observations of the surface number density of SMGs, as can be seen in Fig. 3 where SMG surface number densities of different submm surveys are plotted against rms. Toft et al. (2014) found that at $z \geq 3$ the surface density of bright SMGs is $60 \pm 10 \text{ deg}^{-2}$ to a depth of $1.3 \text{ mJy beam}^{-1}$

¹ SMGs were historically defined by having a submm flux density of $S_{850 \mu\text{m}} > 2 \text{ mJy}$. SMGs are massive gas-rich, high-redshift galaxies with high-IR luminosities, $L_{\text{IR}} \geq 10^{12} L_\odot$, believed to be from starburst activity, with star formation rates (SFRs) of several 100 – $1000 M_\odot \text{ yr}^{-1}$ (Smail, Ivison & Blain 1997; Ivison et al. 1998; Eales et al. 1999; Smail et al. 2000; Blain et al. 2002; Pope et al. 2006; Casey et al. 2014; Swinbank et al. 2014). SMGs are enshrouded by dust and hence are faint in optical and near-IR wavelengths.

Table 1. Coordinates and photometry of the 17 companion SMG sources found around 10 Hot DOGs, with 3.4, 4.6, 12 and 22 μm magnitudes from the AllWISE Source Catalog and 850 μm flux densities from SCUBA-2. The targets with WISE upper limits have SNR < 2 and therefore in the AllWISE Source Catalog the magnitudes quoted are 2σ upper limits. The top six WISE-selected Hot DOGs are detected at 850 μm , while the bottom four Hot DOGs have upper limits at 850 μm . No *Herschel*, NVSS, FIRST data and no objects found in SIMBAD for all the 17 companion SMG sources. FIRST detection limit for each source position is given in mJy beam^{-1} , ‘undetected’ represents that there is no FIRST coverage or NVSS detection. A search radius of 8 arcsec was used, which is a typical search radius of SMG counterparts (Hainline et al. 2009).

Source name	RA (J2000)	Dec. (J2000)	Distance to WISE target (arcsec)	WISE name (mag)	3.4 μm (mag)	4.6 μm (mag)	12 μm (mag)	22 μm (mJy)	850 μm	SNR	FIRST /NVSS detection limit (mJy beam^{-1})
W0831+0140-1	08:31:49.565	01:41:10.80	78 \pm 8	WISE undetected	N/A	N/A	N/A	N/A	6.4 \pm 2.1	3.0	1.00
W0831+0140-2	08:31:48.498	01:40:30.80	73 \pm 7	WISE undetected	N/A	N/A	N/A	N/A	7.7 \pm 2.1	3.7	0.99
W0831+0140-3	08:31:50.899	01:39:58.80	32 \pm 3	WISE undetected	N/A	N/A	N/A	N/A	6.9 \pm 2.1	3.3	0.99
W1136+4236-1	11:36:32.868	42:35:14.42	48 \pm 5	WISE undetected	N/A	N/A	N/A	N/A	5.4 \pm 1.7	3.2	1.06
W1603+2747-1 ^a	16:03:59.222	27:47:05.48	70 \pm 7	WISE undetected	N/A	N/A	N/A	N/A	6.8 \pm 1.8	3.8	0.93
W1835+4355-1 ^a	18:35:28.518	43:54:52.36	77 \pm 8	WISE undetected	N/A	N/A	N/A	N/A	4.6 \pm 1.5	3.1	Undetected
W2216+0723-1 ^a	22:16:21.520	07:24:06.50	30 \pm 3	WISE undetected	N/A	N/A	N/A	N/A	4.9 \pm 1.6	3.1	0.80
W2216+0723-2 ^a	22:16:16.142	07:24:34.83	33 \pm 3	WISE undetected	N/A	N/A	N/A	N/A	5.3 \pm 1.6	3.3	0.79
W2246-0526-1	22:46:02.433	-05:26:35.43	74 \pm 7	WISE undetected	N/A	N/A	N/A	N/A	6.9 \pm 2.1	3.3	0.97
W1814+3412-1 ^b	18:14:23.130	34:12:01.79	67 \pm 7	J181423.13+341205.2	16.848 \pm 0.080	16.748 \pm 0.243	12.153 \pm 0.283	<8.791	5.4 \pm 1.8	3.0	Undetected
W2026+0716-1	20:26:16.913	07:15:55.7	37 \pm 4	J202616.55+071600.6	15.336 \pm 0.038	15.259 \pm 0.085	<12.781	<9.034	7.3 \pm 1.7	4.3	Undetected
W2026+0716-2	20:26:20.139	07:17:03.57	72 \pm 7	WISE undetected	N/A	N/A	N/A	N/A	6.1 \pm 1.7	3.6	Undetected
W2054+0207-1	20:54:22.159	02:06:48.38	18 \pm 2	WISE undetected	N/A	N/A	N/A	N/A	6.9 \pm 1.8	3.8	0.96
W2054+0207-2	20:54:24.376	02:06:46.54	16 \pm 2	WISE undetected	N/A	N/A	N/A	N/A	5.6 \pm 1.8	3.1	0.96
W2054+0207-3	20:54:29.713	02:06:19.15	68 \pm 7	WISE undetected	N/A	N/A	N/A	N/A	6.8 \pm 1.8	3.8	0.98
W2357+0328-1	23:57:08.930	03:27:11.40	48 \pm 5	J235708.59+032712.1	17.574 \pm 0.212	16.679 \pm 0.375	<12.031	<8.677	5.8 \pm 1.9	3.1	0.86
W2357+0328-2	23:57:05.457	03:27:11.40	84 \pm 8	J235705.39+032710.3	16.536 \pm 0.084	16.177 \pm 0.240	<11.869	<8.856	6.7 \pm 1.9	3.5	0.86

^aSubset of these Hot DOGs have been reported by Tsai et al. (2015).

^bSubset of these Hot DOGs have been reported by Eisenhardt et al. (2012).

Table 2. Coordinates and photometry of the 81 companion SMG sources found around 30 *WISE*/radio AGNs, with 3.4, 4.6, 12 and 22 μm magnitudes from the AllWISE Source Catalog and 850 μm flux densities from SCUBA-2. The targets with *WISE* upper limits have SNR < 2 and therefore in the AllWISE Source Catalog the magnitudes quoted are 2σ upper limits. No *Herschel*, NVSS, FIRST data and no objects found in SIMBAD for all the 81 companion SMG sources. FIRST detection limit for each source position is given in mJy beam^{-1} , ‘undetected’ represents that there is no FIRST coverage or NVSS detection. A search radius of 8 arcsec was used, which is a typical search radius of SMG counterparts (Hainline et al. 2009).

Source name	RA (J2000)	Dec. (J2000)	Distance to <i>WISE</i> target (arcsec)	<i>WISE</i> name	3.4 μm (mag)	4.6 μm (mag)	12 μm (mag)	22 μm (mag)	850 μm (mJy)	SNR	FIRST /NVSS detection limit (mJy beam $^{-1}$)
W0010+1643-1	00:10:41.983	16:43:44.70	32 \pm 3	<i>WISE</i> undetected	N/A	N/A	N/A	N/A	6.0 \pm 1.9	3.2	Undetected
W0010+1643-2	00:10:42.284	16:43:28.70	36 \pm 4	J001042.69+164333.2	16.349 \pm 0.071	16.116 \pm 0.183	<11.970	<9.008	5.9 \pm 1.9	3.1	Undetected
W0010+1643-3	00:10:40.614	16:42:52.37	34 \pm 4	J001040.14+164253.2	16.876 \pm 0.108	16.268 \pm 0.228	<11.943	<8.720	5.7 \pm 1.9	3.0	Undetected
W0010+1643-4	00:10:36.461	16:42:16.37	23 \pm 3	J001036.63+164217.1	17.564 \pm 0.187	16.550 \pm 0.295	<12.102	<8.791	6.5 \pm 1.9	3.4	Undetected
W0244+1123-1	02:44:23.184	11:24:58.40	58 \pm 6	<i>WISE</i> undetected	N/A	N/A	N/A	N/A	7.9 \pm 2.1	3.8	Undetected
W0244+1123-2	02:44:20.191	11:24:58.40	76 \pm 7	<i>WISE</i> undetected	N/A	N/A	N/A	N/A	6.6 \pm 2.1	3.1	Undetected
W0244+1123-3	02:44:19.942	11:24:10.40	68 \pm 7	J024419.14+112416.0 9	14.860 \pm 0.032	14.546 \pm 0.051	<12.121	<9.261	6.4 \pm 2.1	3.0	Undetected
W0244+1123-4	02:44:19.942	11:23:10.06	74 \pm 7	<i>WISE</i> undetected	N/A	N/A	N/A	N/A	6.9 \pm 2.1	3.3	Undetected
W0332+3205-1	03:32:28.489	32:05:28.67	21 \pm 3	J033228.76+320525.3	16.032 \pm 0.061	16.060 \pm 0.190	<12.561	<8.833	10.4 \pm 2.0	5.2	Undetected
W0332+3205-2	03:32:34.155	32:05:48.99	69 \pm 7	<i>WISE</i> undetected	N/A	N/A	N/A	N/A	6.5 \pm 2.0	3.3	Undetected
W0342+3753-1	03:42:23.576	37:54:37.60	60 \pm 6	J034223.52+375442.8	14.520 \pm 0.030	14.523 \pm 0.055	<11.797	<8.743	8.8 \pm 2.1	4.2	Undetected
W0342+3753-2	03:42:22.562	37:54:22.93	32 \pm 4	<i>WISE</i> undetected	N/A	N/A	N/A	N/A	6.6 \pm 2.1	3.1	Undetected
W0342+3753-3	03:42:20.872	37:54:26.27	52 \pm 5	<i>WISE</i> undetected	N/A	N/A	N/A	N/A	7.0 \pm 2.1	3.3	Undetected
W0342+3753-4	03:42:16.170	37:53:45.92	78 \pm 8	J034216.58+375348.5	17.429 \pm 0.167	<16.701	<12.640	<8.999	6.9 \pm 2.1	3.3	Undetected
W0342+3753-5	03:42:28.278	37:52:58.26	58 \pm 6	<i>WISE</i> undetected	N/A	N/A	N/A	N/A	8.6 \pm 2.1	4.1	Undetected
W0342+3753-6	03:42:28.644	37:53:26.26	57 \pm 6	<i>WISE</i> undetected	N/A	N/A	N/A	N/A	7.6 \pm 2.1	3.6	Undetected
W0342+3753-7	03:42:20.872	37:53:58.27	34 \pm 4	J034221.22+375401.9	15.911 \pm 0.056	16.036 \pm 0.167	<11.844	<8.938	7.4 \pm 2.1	3.5	Undetected
W0352+1947-1	03:52:09.368	19:47:08.86	54 \pm 5	<i>WISE</i> undetected	N/A	N/A	N/A	N/A	6.0 \pm 1.9	3.2	Undetected
W0404+0712-1	04:04:41.751	07:12:59.20	40 \pm 4	J040441.89+071258.0	17.185 \pm 0.145	<17.301	<12.608	<9.134	6.2 \pm 1.9	3.3	Undetected
W0404+0712-2	04:04:43.566	07:12:30.20	35 \pm 4	<i>WISE</i> undetected	N/A	N/A	N/A	N/A	6.1 \pm 1.9	3.2	Undetected
W0443+0643-1	04:43:32.581	06:43:50.10	32 \pm 4	<i>WISE</i> undetected	N/A	N/A	N/A	N/A	13.5 \pm 3.7	3.6	Undetected
W0443+0643-2	04:43:34.230	06:42:09.81	68 \pm 7	J044334.58+064212.9	15.757 \pm 0.049	15.578 \pm 0.140	<12.240	<8.843	12.0 \pm 3.7	3.2	Undetected
W0443+0643-3	04:43:35.534	06:42:18.67	70 \pm 7	<i>WISE</i> undetected	N/A	N/A	N/A	N/A	6.0 \pm 1.9	3.2	Undetected
W0849+3033-1	08:49:02.961	30:32:33.00	62 \pm 6	<i>WISE</i> undetected	N/A	N/A	N/A	N/A	7.7 \pm 2.4	3.2	0.93

Table 3. Continue table of coordinates and photometry of the 81 companion SMG sources found around 30 WISE/radio AGNs, with 3.4, 4.6, 12 and 22 μm magnitudes from the AllWISE Source Catalog and 850 μm flux densities from SCUBA-2. The targets with WISE upper limits have SNR < 2 and therefore in the AllWISE Source Catalog the magnitudes quoted are 2σ upper limits. No *Herschel*, NVSS, FIRST data and no objects found in SIMBAD for all the 81 companion SMG sources. FIRST detection limit for each source position is given in mJy beam $^{-1}$, ‘undetected’ represents that there is no FIRST coverage or NVSS detection. A search radius of 8 arcsec was used, which is a typical search radius of SMG counterparts (Hainline et al. 2009).

Source name	RA (J2000)	Dec. (J2000)	Distance to WISE target (arcsec)	WISE name	3.4 μm (mag)	4.6 μm (mag)	12 μm (mag)	22 μm (mag)	850 μm (mJy)	SNR	FIRST /NVSS detection limit (mJy beam $^{-1}$)
W0849+3033-2	08:49:05.438	30:32:12.33	76 \pm 8	WISE undetected	N/A	N/A	N/A	N/A	7.5 \pm 2.4	3.1	0.93
W0849+3033-3	08:49:07.270	30:32:12.33	83 \pm 8	WISE undetected	N/A	N/A	N/A	N/A	7.9 \pm 2.4	3.3	0.92
W1025+6128-1	10:25:02.081	61:28:49.02	54 \pm 5	WISE undetected	N/A	N/A	N/A	N/A	6.3 \pm 2.0	3.2	0.98
W1025+6128-2	10:25:12.691	61:27:40.36	58 \pm 6	WISE undetected	N/A	N/A	N/A	N/A	6.0 \pm 2.0	3.0	0.98
W1025+6128-3	10:25:14.969	61:27:21.36	78 \pm 8	WISE undetected	N/A	N/A	N/A	N/A	6.1 \pm 2.0	3.1	0.98
W1046-0250-1	10:46:31.465	-02:50:06.70	30 \pm 4	J104631.08-025001.8	17.645 \pm 0.216	16.490 \pm 0.283	<12.532	<8.979	6.7 \pm 2.1	3.2	0.90
W1046-0250-2	10:46:30.931	-02:49:11.03	75 \pm 8	WISE undetected	N/A	N/A	N/A	N/A	7.2 \pm 2.1	3.4	0.90
W1046-0250-3	10:46:37.272	-02:50:32.70	59 \pm 6	WISE undetected	N/A	N/A	N/A	N/A	6.2 \pm 2.1	3.0	0.90
W1107+3421-1	11:07:32.012	34:20:55.03	34 \pm 4	WISE undetected	N/A	N/A	N/A	N/A	7.0 \pm 2.0	3.0	0.89
W1107+3421-2	11:07:30.425	34:19:51.36	88 \pm 8	WISE undetected	N/A	N/A	N/A	N/A	6.4 \pm 2.0	3.2	0.90
W1210+4750-1	12:10:30.748	47:50:51.20	49 \pm 5	J121031.00+475052.0	17.411 \pm 0.141	16.638 \pm 0.254	<12.681	<8.527	8.2 \pm 2.3	3.6	0.96
W1210+4750-2	12:10:37.038	47:50:30.51	88 \pm 8	WISE undetected	N/A	N/A	N/A	N/A	7.0 \pm 2.3	3.0	0.96
W1210+4750-3	12:10:30.515	47:49:50.86	28 \pm 3	J121030.53+474956.7	16.952 \pm 0.095	16.452 \pm 0.203	<12.641	<9.071	7.6 \pm 2.3	3.3	0.97
W1210+4750-4	12:10:26.676	47:48:38.87	85 \pm 8	J121027.36+474837.9	17.364 \pm 0.129	17.296 \pm 0.468	<12.331	<8.509	10.7 \pm 2.3	4.7	0.95
W1210+4750-5	12:10:21.181	47:49:27.85	75 \pm 8	J121021.04+474927.4	17.210 \pm 0.124	16.402 \pm 0.207	<12.546	<8.992	7.7 \pm 2.3	3.3	0.99
W1212+4659-1	12:12:08.419	47:00:07.23	36 \pm 4	J121208.25+470004.4	16.950 \pm 0.103	16.375 \pm 0.211	<12.261	<8.896	7.9 \pm 2.5	3.2	0.99
W1212+4659-2	12:12:10.015	46:59:34.56	48 \pm 5	WISE undetected	N/A	N/A	N/A	N/A	6.0 \pm 1.9	3.2	0.98
W1212+4659-3	12:12:11.970	46:59:42.22	63 \pm 6	WISE undetected	N/A	N/A	N/A	N/A	7.8 \pm 2.5	3.1	1.58
W1409+1732-1	14:09:22.400	17:32:20.03	82	WISE undetected	N/A	N/A	N/A	N/A	6.4 \pm 2.0	3.2	1.58
W1409+1732-2	14:09:26.832	17:31:44.35	30 \pm 4	J140927.37+173142.7	17.603 \pm 0.174	<16.764	12.961 \pm 0.526	<8.759	6.4 \pm 2.0	3.2	1.58
W1409+1732-3	14:09:27.950	17:31:07.73	59 \pm 6	J140928.23+173108.2	17.956 \pm 0.211	16.908 \pm 0.311	<12.657	<9.339	7.9 \pm 2.0	4.0	0.93
W1428+1113-1	14:29:00.256	17:12:11.25	68 \pm 7	WISE undetected	N/A	N/A	N/A	N/A	6.0 \pm 1.9	3.7	1.0
W1501+1324-1	15:01:41.713	13:24:57.90	44 \pm 4	J150141.93+132450.8	18.011 \pm 0.214	<17.207	<12.892	<9.321	7.1 \pm 2.2	3.2	0.95
W1501+1324-2	15:01:42.192	13:23:57.23	63 \pm 6	J150142.45+132358.6	17.196 \pm 0.106	16.988 \pm 0.330	<12.984	<9.239	7.2 \pm 2.2	3.3	0.94

Table 4. Continue table of coordinates and photometry of the 81 companion SMG sources found around 30 *WISE*/radio AGNs, with 3.4, 4.6, 12 and 22 μm magnitudes from the ALLWISE Source Catalog and 850 μm flux densities from SCUBA-2. The targets with *WISE* upper limits have SNR < 2 and therefore in the ALLWISE Source Catalog the magnitudes quoted are 2σ upper limits. No *Herschel*, NVSS, FIRST data and no objects found in SIMBAD for all the 81 companion SMG sources. FIRST detection limit for each source position is given in mJy beam^{-1} , ‘undetected’ represents that there is no FIRST coverage or NVSS detection. A search radius of 8 arcsec was used, which is a typical search radius of SMG counterparts (Hamline et al. 2009).

Source name	RA (J2000)	Dec. (J2000)	Distance to <i>WISE</i> target (arcsec)	<i>WISE</i> name	3.4 μm (mag)	4.6 μm (mag)	12 μm (mag)	22 μm (mag)	850 μm (mJy)	SNR	FIRST /NVSS detection limit (mJy beam^{-1})
W1501+1324-3	15:01:40.022	13:23:33.90	76 \pm 7	<i>WISE</i> undetected	N/A	N/A	N/A	N/A	7.3 \pm 2.2	3.3	0.94
W1501+1324-4	15:01:38.423	13:24:33.57	20 \pm 3	<i>WISE</i> undetected	N/A	N/A	N/A	N/A	6.8 \pm 2.2	3.1	0.94
W1517+3523-1	15:17:59.282	35:24:29.97	32 \pm 3	<i>WISE</i> undetected	N/A	N/A	N/A	N/A	5.8 \pm 1.9	3.1	0.94
W1517+3523-2	15:17:56.992	35:23:49.97	24 \pm 3	<i>WISE</i> undetected	N/A	N/A	N/A	N/A	5.7 \pm 1.9	3.0	0.99
W1517+3523-3	15:17:51.703	35:23:33.95	88 \pm 8	J151751.39+352327.9	17.874 \pm 0.158	<17.702	<12.762	<9.464	5.7 \pm 1.9	3.0	0.99
W1517+3523-4	15:17:54.348	35:23:02.30	72 \pm 7	J151754.19+352302.8	16.418 \pm 0.052	15.611 \pm 0.084	12.607 \pm 0.319	<9.495	5.7 \pm 1.9	3.0	0.99
W1517+3523-5	15:17:56.065	35:22:35.30	74 \pm 7	<i>WISE</i> undetected	N/A	N/A	N/A	N/A	5.8 \pm 1.9	3.1	0.99
W1630+5126-1	16:30:41.014	51:26:52.03	56 \pm 6	<i>WISE</i> undetected	N/A	N/A	N/A	N/A	5.8 \pm 1.9	3.1	0.96
W1630+5126-2	16:30:30.174	51:27:04.36	73 \pm 7	<i>WISE</i> undetected	N/A	N/A	N/A	N/A	5.8 \pm 1.9	3.1	0.97
W1703+2615-1	17:03:35.673	26:16:19.28	70 \pm 7	<i>WISE</i> undetected	N/A	N/A	N/A	N/A	6.8 \pm 2.0	3.4	0.98
W1717+5313-1	17:17:00.517	53:13:51.29	49 \pm 5	<i>WISE</i> undetected	N/A	N/A	N/A	N/A	7.5 \pm 2.5	3.0	0.95
W1717+5313-2	17:17:00.592	53:13:15.63	53 \pm 5	J171700.48+531319.7	15.618 \pm 0.341	15.988 \pm 0.195	<10.482	<8.604	11.7 \pm 2.5	4.7	0.95
W1717+5313-3	17:17:08.461	53:13:15.96	40 \pm 4	<i>WISE</i> undetected	N/A	N/A	N/A	N/A	7.5 \pm 2.5	3.0	0.96
W2126-0103-1	21:26:17.587	-01:04:18.48	50 \pm 5	<i>WISE</i> undetected	N/A	N/A	N/A	N/A	7.8 \pm 2.0	3.9	1.0
W2133-1419-1	21:33:53.760	-14:19:46.42	58 \pm 6	J213353.65-141946.5	15.002 \pm 0.037	14.929 \pm 0.080	<12.506	<8.595	5.5 \pm 1.8	3.1	Undetected
W2212+3326-1	22:12:54.092	33:26:36.35	63 \pm 6	<i>WISE</i> undetected	N/A	N/A	N/A	N/A	8.9 \pm 2.0	4.5	Undetected
W2212+3326-2	22:13:01.443	33:27:24.72	86 \pm 8	<i>WISE</i> undetected	N/A	N/A	N/A	N/A	6.7 \pm 2.0	3.4	Undetected
W2212-1253-1	22:12:00.655	-12:53:38.03	59 \pm 6	<i>WISE</i> undetected	N/A	N/A	N/A	N/A	8.0 \pm 2.1	3.8	Undetected
W2212-1253-2	22:12:09.226	-12:54:07.70	59 \pm 6	<i>WISE</i> undetected	N/A	N/A	N/A	N/A	7.5 \pm 2.1	3.6	Undetected
W2222+0951-1	22:22:44.211	09:51:18.11	58 \pm 6	<i>WISE</i> undetected	N/A	N/A	N/A	N/A	7.3 \pm 2.0	3.7	0.86
W2222+0951-2	22:22:46.971	09:50:09.38	78 \pm 7	J222247.42+095008.1	17.476 \pm 0.180	<17.290	<12.598	<8.629	9.3 \pm 2.0	4.7	0.85
W2222+0951-3	22:22:50.953	09:50:29.02	62 \pm 6	<i>WISE</i> undetected	N/A	N/A	N/A	N/A	8.6 \pm 2.0	4.3	0.86
W2226+0025-1	22:26:20.255	00:24:35.57	69 \pm 7	<i>WISE</i> undetected	N/A	N/A	N/A	N/A	8.4 \pm 1.9	4.4	0.77
W2226+0025-2	22:26:21.855	00:24:04.23	74 \pm 7	<i>WISE</i> undetected	N/A	N/A	N/A	N/A	6.9 \pm 1.9	3.7	0.77

Table 5. Continue table of coordinates and photometry of the 81 companion SMG sources found around 30 WISE/radio AGNs, with 3.4, 4.6, 12 and 22 μm magnitudes from the AllWISE Source Catalog and 850 μm flux densities from SCUBA-2. The targets with WISE upper limits have SNR < 2 and therefore in the AllWISE Source Catalog the magnitudes quoted are 2σ upper limits. No *Herschel*, NVSS, FIRST data and no objects found in SIMBAD for all the 81 companion SMG sources. FIRST detection limit for each source position is given in mJy beam^{-1} , ‘undetected’ represents that there is no FIRST coverage or NVSS detection. A search radius of 8 arcsec was used, which is a typical search radius of SMG counterparts (Hainline et al. 2009).

Source name	RA (J2000)	Dec. (J2000)	Distance to WISE target (arcsec)	WISE name	3.4 μm (mag)	4.6 μm (mag)	12 μm (mag)	22 μm (mag)	850 μm (mJy)	SNR	FIRST /NVSS detection limit (mJy beam^{-1})
W2230-0720-1	22:30:06.993	-07:19:51.90	70 \pm 7	WISE undetected	N/A	N/A	N/A	N/A	5.8 \pm 1.8	3.2	0.93
W2230-0720-2	22:30:09.189	-07:19:59.90	57 \pm 6	WISE undetected	N/A	N/A	N/A	N/A	6.0 \pm 1.8	3.3	0.93
W2230-0720-3	22:30:12.080	-07:20:47.90	59 \pm 6	WISE undetected	N/A	N/A	N/A	N/A	5.5 \pm 1.8	3.1	0.93
W2230-0720-4	22:30:08.607	-07:22:24.23	80 \pm 8	J223008.35-072220.9	17.423 \pm 0.174	16.992 \pm 0.438	<12.065	<8.834	5.7 \pm 1.8	3.2	0.92
W2325-0429-1	23:25:06.972	-04:28:44.43	66 \pm 7	WISE undetected	N/A	N/A	N/A	N/A	7.1 \pm 2.1	3.4	2.27
W2325-0429-2	23:25:01.088	-04:30:43.77	76 \pm 7	WISE undetected	N/A	N/A	N/A	N/A	9.8 \pm 2.1	4.7	2.20
W2331-1411-1	23:31:05.148	-14:11:08.87	48 \pm 5	J233104.89-141108.4	16.393 \pm 0.074	16.900 \pm 0.423	<12.543	<8.351	6.9 \pm 2.2	3.1	Undetected
W2345+3120-1	23:45:44.634	31:19:41.80	56 \pm 6	J234544.45+311941.9	17.217 \pm 0.124	15.988 \pm 0.157	<12.585	<8.841	11.3 \pm 2.0	5.7	Undetected
W2345+3120-2	23:45:34.358	31:20:02.12	84 \pm 8	WISE undetected	N/A	N/A	N/A	N/A	6.3 \pm 2.0	3.2	Undetected

Table 6. SFRDs of Hot DOGs (top 10) and WISE/radio AGNs (bottom 30) and their surrounding SMGs, assuming that they are at the same redshift. The angular radius is estimated to be the size of the SCUBA-2 map, 1.5 arcmin. The spectroscopically known redshifts of the WISE-selected targets are shown. The unknown redshifts of the WISE/radio AGNs are assumed to be the average of WISE/radio AGNs, $z = 1.7$.

Source	SFRD ($\text{M}_{\odot} \text{yr}^{-1} \text{Mpc}^{-3}$)	Redshift
W0831+0140	7949 \pm 159	3.91
W1136+4236	2064 \pm 41	2.39
W1603+2747	2989 \pm 60	2.63
W1814+3412	1523 \pm 30	2.45
W1835+4355	2406 \pm 48	2.3
W2026+0716	2835 \pm 57	2.54
W2054+0207	4304 \pm 86	2.52
W2216+0723	2917 \pm 58	1.68
W2246-0526	5808 \pm 116	4.59
W2357+0328	2538 \pm 51	2.12
W0010+1643	5311 \pm 106	2.855
W0244+1123	4035 \pm 162	Unknown
W0332+3205	1799 \pm 72	Unknown
W0342+3753	18715 \pm 374	0.47
W0352+1947	1045 \pm 42	Unknown
W0404+0712	2133 \pm 85	Unknown
W0443+0643	3686 \pm 147	Unknown
W0849+3033	4005 \pm 160	Unknown
W1025+6128	3091 \pm 124	Unknown
W1046-0250	2699 \pm 108	Unknown
W1107+3421	2119 \pm 42	Unknown
W1210+4750	4992 \pm 100	Unknown
W1212+4659	3178 \pm 64	Unknown
W1409+1732	3454 \pm 138	Unknown
W1428+1113	1219 \pm 49	1.6
W1501+1324	9501 \pm 190	0.505
W1517+3523	4499 \pm 90	1.515
W1630+5126	2046 \pm 82	Unknown
W1703+2615	1364 \pm 55	Unknown
W1717+5313	3935 \pm 157	2.717
W2126-0103	2247 \pm 89	0.607
W2133-1419	1132 \pm 45	Unknown
W2212-1253	2931 \pm 117	Unknown
W2212+3326	1799 \pm 72	Unknown
W2222+0951	3149 \pm 63	Unknown
W2226+0025	4025 \pm 80	0.607
W2230-0720	12596 \pm 252	0.444
W2325-0429	2220 \pm 88	1.737
W2331-1411	2177 \pm 87	Unknown
W2345+3120	2772 \pm 111	Unknown

(submm interferometry), which was found to be ~ 30 per cent lower than $z \sim 2$ quiescent galaxies. SMGs from the LABOCA-COSMOS survey were found to have a surface density between 34 ± 14 and $54 \pm 18 \text{ deg}^{-2}$ at a depth of $1.5 \text{ mJy beam}^{-1}$ (submm interferometry), which was higher than models predicted (Smolčić et al. 2012). In the GOODS-N field, the surface density of SMGs was found to be $\geq 87 \text{ deg}^{-2}$ (Pope et al. 2005) at depths ranging from 0.3 to $4.1 \text{ mJy beam}^{-1}$ (submm single dish). This was likely higher than previous observations due to the association with a protocluster at $z \sim 4.05$. Geach et al. (2017) found a tentative overdensity in the GOODS-N compared to the rest of the SCUBA-2 Cosmology Legacy Survey (S2CLS), while combining all of the S2CLS fields, the number counts are consistent with previous studies. Fig. 3 also visually highlights the difference in rms between single dish and interferometer measurements.

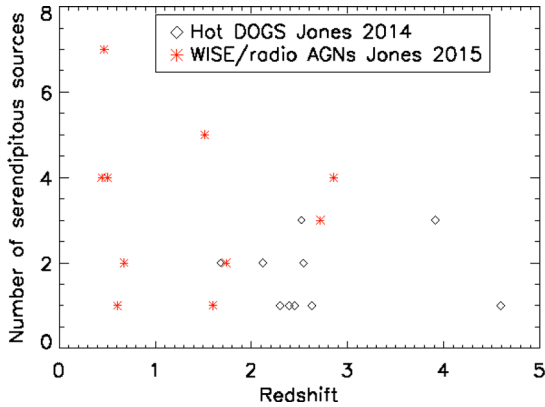


Figure 1. The number of submm companion sources found in each of the 10 Hot DOG fields with known redshifts (Jones et al. 2014), and the 10 *WISE*/radio-selected AGN fields with known redshifts (Jones et al. 2015), are shown by black diamonds and red asterisks, respectively. From previous blank-field submm surveys ~ 1 companion source is expected in each 1.5-arcmin radius SCUBA-2 field.

The space density of SMGs in the Hot DOG fields on average is 3.7 Mpc^{-3} (range $3.0\text{--}6.2 \text{ Mpc}^{-3}$), and in the *WISE*/radio AGN fields the average space density is 2.9 Mpc^{-3} (range $0.7\text{--}15 \text{ Mpc}^{-3}$). These space densities are higher than normal star-forming galaxies ($\sim 2 \times 10^{-4} \text{ Mpc}^{-3}$) and local luminous red galaxies ($\sim 10^{-4} \text{ Mpc}^{-3}$) (Wake et al. 2008). Previous studies have found SMGs have low number densities of $\sim 1\text{--}2 \times 10^{-5} \text{ Mpc}^{-3}$, and are consistent across all redshifts (Wilkinson et al. 2017). The S2CLS was found to have SMG number densities between 4×10^{-5} and $2 \times 10^{-4} \text{ Mpc}^{-3}$. This confirms that the fields around Hot DOGs and *WISE*/radio AGNs are overdense compared to previous studies of SMGs and normal star-forming galaxies.

3 TWO-POINT CORRELATION FUNCTION

The angular two-point correlation function $\omega(\theta)$ is a statistical way to characterize the clustering of galaxies in two-dimensional (2D) space (Efstathiou et al. 1991; Connolly, Szalay & Brunner 1998). We detect galaxies on a 2D surface and hence we use the angular version of the 3D spatial correlation function (Peebles 1980). It is the excess probability of finding galaxies separated by θ as compared with a random distribution. Using the one of the popular estimators described by Landy & Szalay (1993)

$$\omega(\theta) = (|DD| - 2 \times |DR| + |RR|)/|RR| + \sigma^2,$$

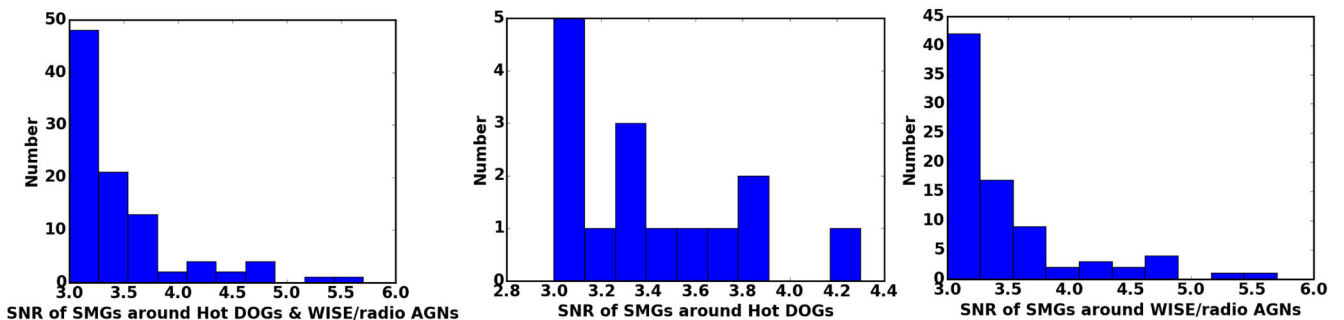


Figure 2. Three histograms to show the distribution of SNR of the companion sources detected around Hot DOGs (right), *WISE*/radio AGN (centre) and combining both sets (left).

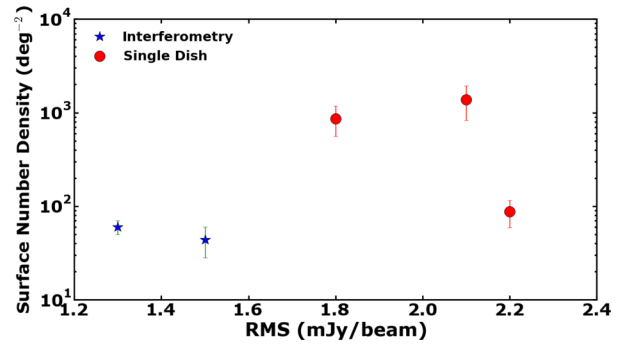


Figure 3. The surface number density of SMGs against rms in the Hot DOG and *WISE*/radio AGN fields are shown in red circles, in comparison to the GOODS-N field single submm dish observations (Pope et al. 2005) also in red circles. The blue stars are submm interferometry observations of SMGs by Toft et al. (2014) and Smolčić et al. (2012). The surface number density of the Hot DOG and *WISE*/radio AGN fields are higher than previous submm surveys.

where $\omega(\theta)$ is the angular correlation function, DD is the number of pairs of galaxies counted in the sample, RR is the number of pairs of galaxies expected in a random distribution, DR is the number of pairs of galaxies counted between the sample and a random distribution and σ is the integral constraint (Groth & Peebles 1977). The counts have been normalized by dividing by the total number of pairs in each of the three samples; DD, DR and RR.

The angular correlation function was calculated for the 30 *WISE*/radio-selected AGN fields. It was not calculated for the Hot DOG fields because there were only 10 fields and not a large enough number of companion sources to be statistically significant: the errors would be greater than the large errors on the 30 *WISE*/radio AGNs. To calculate the angular correlation function, 100 000 random fake galaxies were used and compared with the blank-field survey from Weiß et al. (2009), which investigated clustering of faint galaxies, see Fig. 4. Weiß et al. (2009) found significant clustering on scales less than 1 arcmin and a characteristic angular clustering scale $\theta_0 = 14 \text{ arcmin} \pm 7 \text{ arcsec}$ and a spatial correlation length of $r_0 = 13 \pm 6 h^{-1} \text{ Mpc}$. We also compared to Wilkinson et al. (2017) that analysed the largest sample of SMGs (610) in a single field to date from the S2CLS in the redshift range $1 < z < 3$. They found a marginally weaker clustering signal than previous studies, but within 1σ uncertainty the results are consistent with Blain et al. (2004), Adelberger et al. (2005) and Hickox et al. (2012). They also concluded that radio-selected SMGs were slightly more strongly clustered.

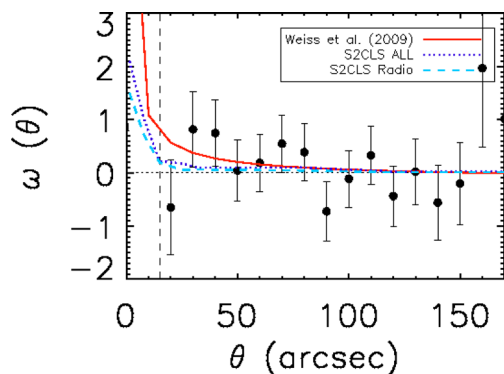


Figure 4. Observed angular two-point correlation function using the Landy & Szalay (1993) equation. The red solid curve shows the observed angular two-point correlation function for Weiß et al. (2009). The blue dotted line and cyan dashed line show the observed angular two-point correlation function for all the SMGs and the subset of radio-detected SMGs, respectively, in the S2CLS (Wilkinson et al. 2017). Black points represent the observed angular two-point correlation function for the companion sources detected around WISE/radio AGNs. The dashed line represents the JCMT SCUBA-2 850- μm beam size (15 arcsec). There were not enough data for reliable results using the Hot DOGs.

It can be seen in Fig. 4 that the results in the WISE/radio AGN fields provide an upper limit to the strength of an angular clustering signal, and yields a clustering angle of $\theta_0 \geq 80$ arcsec. The clustering signal appears to be inconsistent to previous clustering results of SMGs; however, further observations would provide more definite results. The results from Jones et al. (2014, 2015) found no evidence for angular clustering when looking at the cumulative fraction of the total number of companion sources in each field within different radii of the WISE target and when looking at typical separations compared to Monte Carlo simulations.

4 PROPERTIES OF THE COMPANION SOURCES AROUND HOT DOGS AND WISE/RADIO AGNS

4.1 Counterparts of the companion sources

A search radius of half SCUBA-2 850- μm beam size (~ 8 arcsec) was used to find counterparts of these companion SMGs in other catalogues (Lilly et al. 1999; Ivison et al. 2002; Hainline et al. 2009). This search radius is determined from the probability of finding a source at a given distance from the SMG position (Lilly et al. 1999; Ivison et al. 2002). This search radius is relatively large due to the difficulty of identifying SMGs at optical and near-IR wavelengths because of the large submm (SCUBA-2) beam, 15 arcsec at 850 μm (Dempsey et al. 2013).

Multiple objects within the WISE AllWISE Source Catalog had two potential counterparts within the 8 arcsec search radius. To reduce ambiguity in the result, the closest in WISE W1–W4 bands object is chosen while excluding objects that have WISE colours consistent with stars.

4.2 Mid-IR counterparts

The WISE colour–colour ([W2–W3] versus [W1–W2]) plots of the companion sources around Hot DOGs and WISE/radio AGNs are shown in Fig. 5. These plots can separate different populations of galaxies because of the underlying mechanisms present in each,

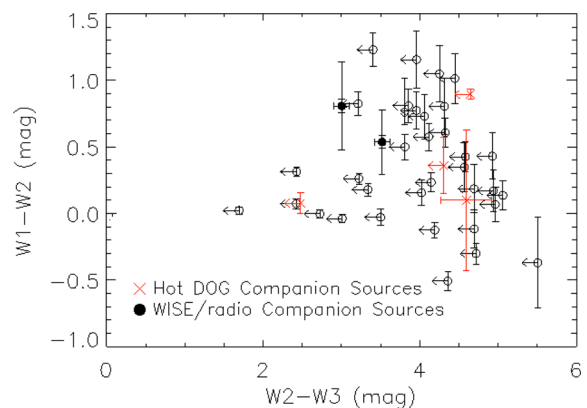


Figure 5. WISE colour–colour [(4.6–12 μm) versus (3.4–4.6 μm) or (W2–W3 versus W1–W2)] plot of the Hot DOGs and WISE/radio AGNs in red crosses and black circles, respectively. Filled circles are detections. When compared with the WISE colour–colour diagram in fig. 12 in Wright et al. (2010) and fig. 26 in Jarrett et al. (2011), the companion sources lie in the starburst zone and appear to be SMGs. They appear to be mid-IR bluer than the Hot DOGs and WISE/radio AGNs.

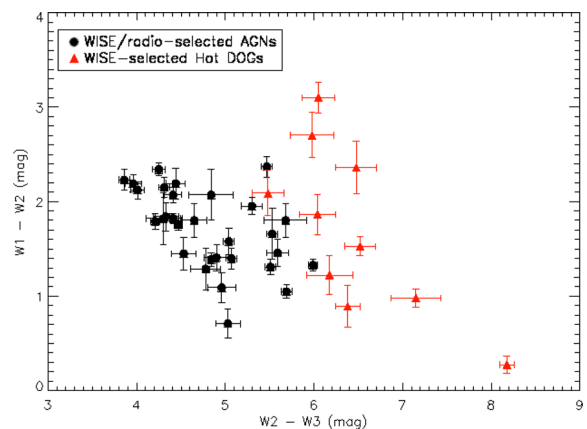


Figure 6. WISE colour–colour [(4.6–12 μm) versus (3.4–4.6 μm) or (W2–W3 versus W1–W2)] plot of the Hot DOGs and WISE/radio AGNs companion sources in red triangles and black circles, respectively. When compared with the WISE colour–colour diagram in fig. 12 in Wright et al. (2010) and fig. 26 in Jarrett et al. (2011), the WISE-selected AGNs are extremely red compared to other galaxy populations.

leading to different mid-IR emission. AGNs are dominated by power-law emission at mid-IR wavelengths. In contrast, normal and star-forming galaxies have a stellar Rayleigh–Jeans tail with additional strong PAH emission, and a continuum that peaks at 70–170 μm due to warm dust heated by young stars (Jarrett et al. 2011).

Both sets of companion sources have similar WISE colours. However, most have upper limits in the W3 band and so have limits to their red W2–W3 colour. When comparing with the WISE colour–colour diagram of different galaxy populations in fig. 12 in Wright et al. (2010) and fig. 26 in Jarrett et al. (2011), the companion sources lie in both the starburst (star-forming) galaxy zone and AGN zone.

The Hot DOGs and WISE/radio AGNs are redder than the companion sources, see Fig. 6. This is no surprise because they were selected to be red (Eisenhardt et al. 2012; Lonsdale et al. 2015), which could imply that they have higher dust obscuration and/or a higher AGN contribution, and higher dust temperatures than that of their companion sources. Hot DOGs and WISE/radio AGNs are

predominantly powered by AGN (Wu et al. 2012; Jones et al. 2014, 2015; Lonsdale et al. 2015; Tsai et al. 2015). SMGs are predominantly powered by star formation (Alexander et al. 2005), and have SEDs dominated by cooler dust emission (20–50 K; Hainline et al. 2009).

Hainline et al. (2009) observed 73 radio-selected SMGs with known redshifts using *Spitzer* IRAC and Multiband Imaging Photometer (MIPS) and detected 91 per cent at 3.6 μm , 91 per cent at 4.5 μm , 78 per cent at 5.8 μm , 74 per cent at 8 μm , 71 per cent at 24 μm and 7 per cent at 70 μm . They found that the detection rate in the shortest bands is less than SMGs in deeper *Spitzer* Wide Area Infrared Extragalactic Legacy Survey (SWIRE). These are higher mid-IR detection rates than the companion SMG sources in the AllWISE Source Catalog presented in this paper (Jones et al. 2015); where 24 and 35 per cent companion SMG sources in the Hot DOG and *WISE*/radio AGN fields, respectively, were detected. The difference in detection rates could be due to the depth of coverage. *Spitzer* IRAC had deeper mid-IR observations with sensitivity ranging from 0.1 to 0.9 μJy at 3.6 μm and 0.4 to 1.8 μJy at 4.5 μm , which are deeper than AllWISE Source Catalog 0.08 mJy at 3.4 μm and 0.11 mJy at 4.6 μm at 2σ .

4.3 Submillimetre emission, SFRs and SFRDs

The average submm flux density of SMGs around Hot DOGs is $S_{850\mu\text{m}} = 6.2 \pm 1.8$ mJy, which is comparable to SMGs around *WISE*/radio AGNs, $S_{850\mu\text{m}} = 7.2 \pm 2.1$ mJy. Submm flux densities provide a reliable measurement of SFR (Alexander et al. 2016). Submm flux densities can be converted to SFRs for SMGs with $z > 1.5$ using

$$\text{SFR}_{850\mu\text{m}} = 200 \times S_{850\mu\text{m}}$$

(Barger et al. 2014). The average SFR is $\simeq 1240 M_{\odot}\text{yr}^{-1}$ for SMGs around *WISE*/radio AGNs, slightly lower than the SFR $\simeq 1460 M_{\odot}\text{yr}^{-1}$ for SMGs around Hot DOGs.

Cosmological simulations predict that overdense regions, $\sim 5\sigma$ density peak, are associated with high SFRs, $\sim 750 M_{\odot}\text{yr}^{-1}$ (Yajima et al. 2015). Observations at redshifts $z \sim 1$ found that higher SFRs are associated with higher densities (Cooper et al. 2007). The mean SFR at the core of protoclusters have been found to be enhanced, up to a factor of ~ 5.9 over the field (Alexander et al. 2016), and outside of the central region the SFR is consistent with field galaxies. ALMA observations of the SSA22 protocluster at redshift $z = 3.09$ found enhanced SFR in the densest regions (Umehata et al. 2015). Therefore, higher SFRs of the SMGs around *WISE*/radio AGNs than the SMGs around Hot DOGs is expected.

The SFRD represents the total star formation transpiring per unit time and volume at a given redshift, as seen in Fig. 6. SFRD allows direct comparison of the importance of IR-luminous galaxies to the build-up of stellar mass in the Universe. From previous work, the SFRD in clusters increases with redshift from $z \sim 1$ to $z \sim 3$ e.g. (Hopkins et al. 2006; Bouwens et al. 2011; Magnelli et al. 2011; Clements et al. 2014), e.g. Dannerbauer et al. (2014) measured an SFRD of $\sim 900 M_{\odot}\text{yr}^{-1}\text{Mpc}^{-3}$ in the field around the spiderweb radio galaxy at redshift $z = 2.16$ in a region of 2 Mpc. However, there are observations of high-redshift clusters with a combination of quiescent and star-forming galaxies (Gobat et al. 2013; Strazzullo et al. 2013), and clusters dominated by quiescent galaxies (Tanaka et al. 2013). Therefore, higher redshift SFRDs are needed to understand the history of galaxy clusters especially in the peak epoch of star formation at redshifts $1 < z < 3$, which includes this paper. The SFRDs were calculated for each cluster, which is the *WISE*-selected

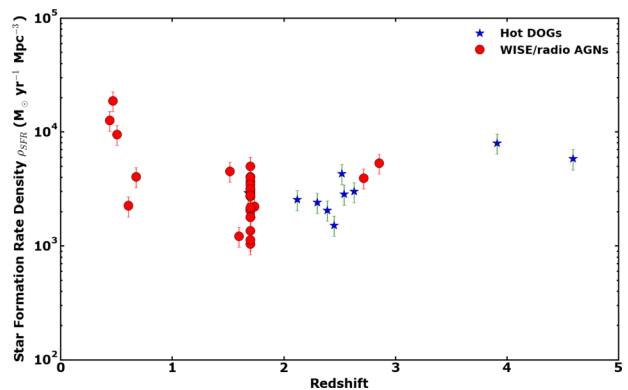


Figure 7. SFRD of each Hot DOG and *WISE*/radio AGN and their surrounding SMGs. The SFRDs are higher than field galaxies and similar to the four HerMES clumps, other clusters with MIR/FIR measurements from the literature, when comparing with fig. 15 from Clements et al. (2014).

source and its surrounding SMGs, assuming that the SMGs are at the same redshift as the source. We assumed that each cluster was spherical, and derived an angular radius from the SCUBA-2 map, 1.5 arcmin. The angular radius was converted to a proper distance at the redshift for each cluster, where the redshift is unknown the average redshift is assumed, $z = 1.7$ for *WISE*/radio AGNs. The volume for each cluster was calculated by assuming that this proper distance is the radius of the cluster. The SFRDs are presented in Table 6, these are lower limits because faint SMGs could be missed due to the shallow depths of the SCUBA-2 maps.

The SFRDs range for Hot DOGs from 1523 ± 30 to $7949 \pm 159 M_{\odot}\text{yr}^{-1}\text{Mpc}^{-3}$, and average $3533 M_{\odot}\text{yr}^{-1}\text{Mpc}^{-3}$. These are lower than *WISE*/radio AGNs with a range from 1219 ± 49 to $18715 \pm 374 M_{\odot}\text{yr}^{-1}\text{Mpc}^{-3}$, and average $3929 M_{\odot}\text{yr}^{-1}\text{Mpc}^{-3}$. Our results in Fig. 7 can be compared to fig. 15 from Clements et al. (2014) and the SFRDs calculated in this paper are higher than field galaxies from Hopkins et al. (2006) and Bouwens et al. (2011), with SFRDs of $\sim 900 M_{\odot}\text{yr}^{-1}\text{Mpc}^{-3}$ and $\sim 700 M_{\odot}\text{yr}^{-1}\text{Mpc}^{-3}$ at $z = 2$, respectively. Our values are similar to four *Herschel* Multitiered Extragalactic Survey (HerMES) clusters of dusty, star-forming galaxies at redshifts between $z = 0.76$ and 2.26, and other clusters with mid-infrared (MIR)/far-infrared (FIR) measurements from the literature with SFRDs ranging from $\sim 200 M_{\odot}\text{yr}^{-1}\text{Mpc}^{-3}$ to $\sim 3000 M_{\odot}\text{yr}^{-1}\text{Mpc}^{-3}$. Simulations of massive galaxy clusters cannot account for the overdensity found by Clements et al. (2014), which is thought to be due to insufficient peaks of star formation activity in the simulations at early epochs, and including strong starbursts in the simulations is required to explain the statistical properties of SMGs (Granato et al. 2015).

Dusty star-forming galaxy (DSFG)-rich protoclusters at redshifts $2 < z < 3$ were shown to have slightly higher SFRDs compared to the field, due to their large occupying volumes (Casey 2016). In contrast virialized clusters at redshifts $z < 1$ have a substantially higher SFRD. This is in agreement with the lower redshift *WISE*-selected AGNs W0342+3753, W1501+1324 and W2230–0720 that have a redshift of $z = 0.47$, 0.505 and 0.444, respectively, and a significantly higher SFRD at 18715 ± 374 , 9501 ± 190 and $12596 \pm 252 M_{\odot}\text{yr}^{-1}\text{Mpc}^{-3}$, respectively. This is due to a high overdensity of SMGs in each field; seven, four and four serendipitous SMG sources in each field, respectively.

Completeness is the rate at which a source is expected to be detected in a map (Hatsukade et al. 2013). It is computed by simulating the detection rate of 1000 fake point sources per flux bin

placed in the real cleaned signal map (Tamura et al. 2009). Brighter SMGs, where the flux density is $S_{1100\ \mu\text{m}} \geq 2.7$ mJy, were found not to be significantly affected from incompleteness and false detections (Tamura et al. 2009). They found that the completeness was ~ 50 per cent at 2.7 mJy and 90 per cent at 4.0 mJy. All the companion sources detected around Hot DOGs and WISE/radio AGNs have flux densities $S_{850\ \mu\text{m}} \geq 4.6$ mJy and $S_{850\ \mu\text{m}} \geq 5.5$ mJy, respectively, see Tables 1–5. The completeness was found to range from 77 to 100 per cent reported by Hatsukade et al. (2013) from 15 SMGs observed. It was concluded that the correction for incompleteness and contamination has an effect on the low flux density bins ($S_{850\ \mu\text{m}} < 2.9$ mJy) and a minimal effect on the high flux density bins ($S_{850\ \mu\text{m}} \geq 2.9$ mJy; Casey et al. 2013). This is also confirmed by Weiß et al. (2009) where the source extraction is complete (> 95 per cent) for sources with flux densities $S_{870\ \mu\text{m}} \geq 6.5$ mJy and 50 per cent complete at ~ 4.0 mJy. Therefore, the SMG completeness of the fields around Hot DOGs and WISE/radio AGNs should be between 50 and 100 per cent complete. Hence the SFRDs could be higher than calculated here. This will also have an effect on the number count comparison with other submm surveys, where the overdensities in the WISE-selected Hot DOG and WISE/radio-selected AGN fields could have an even higher 4.5 overdensity.

4.4 Radio emission

None of the companion sources around Hot DOGs or WISE/radio AGNs were detected at radio wavelengths in FIRST and/or NVSS, where the typical 1.4-GHz detection limit was 1.0 mJy beam $^{-1}$, see Tables 1–5. From previous observations ~ 65 per cent of SMGs with submm flux densities $S_{850\ \mu\text{m}} > 5$ mJy have detectable radio emission in much deeper observations with rms ~ 10 μ Jy (range 2.3–17.4 μ Jy) (Ivison et al. 1998, 2002; Chapman et al. 2005).

None of the 17 or 81 companion sources in the Hot DOG and WISE/radio AGN fields, respectively, are detected in NRAO snapshot follow-up VLA radio maps (Lonsdale, private communication). The non-detections are consistent with SMG SEDs at relevant redshifts.

4.5 X-ray emission

No counterparts to the companion sources from point sources were found in the third XMM-Newton companion source catalogue, 3XMM-DR5 (Rosen et al. 2015). However, previous deeper X-ray observations of SMGs found only 16 with X-ray detections from sample size of 35 (45 ± 8 per cent) (Laird et al. 2009). These observations were from the 2-Ms Chandra survey with flux limits of the order of 10^{-17} erg cm $^{-2}$ s $^{-1}$ and a range 1.1 – 17.7×10^{-16} erg cm $^{-2}$ s $^{-1}$, and are deeper compared with 3XMM-DR5 of the order of 10^{-15} erg cm $^{-2}$ s $^{-1}$ for 3σ detections. Therefore, non-detections from point sources are expected.

5 DISCUSSION

5.1 Companion source clustering

Fig. 4 provides an upper limit to the strength of an angular clustering signal in the WISE/radio AGN fields, and appears to be inconsistent with previous clustering studies of SMGs from Weiß et al. (2009), Hickox et al. (2012) and Wilkinson et al. (2017). Weiß et al. (2009) found consistent correlation length values of SMGs with Blain et al. (2004) and Farrah et al. (2006) but inconsistent with Scott, Dunlop

& Serjeant (2006), this could be explained by the small significance of the clustering signal in both studies.

Hickox et al. (2012) reanalysed SMGs from the LABOCA survey in a novel method to cross-correlate SMGs in the LABOCA survey and galaxies from Spitzer IRAC. They found a lower correlation length, $r_0 = 7.7^{+1.8}_{-2.3} h^{-1}$ Mpc at $z = 2$, than Weiß et al. (2009), but one that is consistent with measurements for optically selected quasars (QSOs). The observed clustering could depend on the submm flux limit of the survey, presence of redshift spikes and uncertainties in redshift selection function (Adelberger et al. 2005; Williams et al. 2011), which could result in uncertainties in clustering estimates. Hickox et al. (2012) compared their autocorrelation length r_0 to previous SMG results with a range of 850- μ m flux limit from 3 to 6 mJy, and found consistent angular clustering estimates. They concluded that SMGs are likely to represent a short-lived transition phase from cold, gas-rich, star-forming galaxies to passively evolving systems.

Wilkinson et al. (2017) found when analysing the largest sample of SMGs in the S2CLS, SMGs are not as strongly clustered as previously thought. However, their measurements were in agreement with previous studies (Blain et al. 2004; Hickox et al. 2012) within 1σ errors, and found a weaker clustering signal when comparing to Weiß et al. (2009). Accounting for blending (Cowley et al. 2015) could bring the previous studies into better agreement with Wilkinson et al. (2017). Alternatively, the SMG clustering could depend on redshift, large-scale environment and merger history. They found that the clustering of SMGs is consistent with star-forming population and lower than passive population at the same redshift, and tentative evidence of halo downsizing. Chapman et al. (2009) proposed that SMGs do not necessarily trace the most massive dark matter haloes.

Donoso et al. (2014) analysed the angular clustering properties of a sample of $\sim 170\ 000$ WISE-selected AGNs with very red mid-IR colours. The whole sample was found to have a similar clustering strength to optically selected quasars at comparable redshifts ($z = 1.1$) in the Sloan Digital Sky Survey (SDSS; Porciani, Magliocchetti & Norberg 2004; Croom et al. 2005; Myers et al. 2007). They are found in denser environments when compared with all SDSS galaxies at that redshift. Redder AGNs that are well detected at $4.6\ \mu\text{m}$ (W2) have a stronger clustering bias (relationship between the distribution of dark matter and luminous matter) than blue AGNs. WISE/SDSS-obscured AGNs are more strongly clustered and inhabit denser environments than unobscured AGNs. DiPompeo et al. (2014) confirmed this but found a smaller difference in angular clustering amplitude between WISE-selected obscured quasars and unobscured quasars. However, Mendez et al. (2016) found no significant difference between obscured and unobscured AGNs.

There is an overdensity of SMGs with approximately two or three SMGs per SCUBA-2 field compared with the expectation of one SMG from blank-field submm surveys. The number of sources for the angular two-point correlation function of Hot DOG and WISE/radio AGN fields were not numerous enough to see an angular clustering signal. Monte Carlo simulations of the typical separation of the companion sources and the cumulative fraction of the total number of companion sources within different radii from the WISE target showed no angular clustering. This is in agreement with Assef et al. (2015), who found no angular dependence of the IRAC overdensities around a subset of Hot DOGs.

From previous evidence there could be clustering on scales greater than the SCUBA-2 fields (Scoville et al. 2000; Blain et al. 2004; Greve et al. 2004; Farrah et al. 2006; Ivison et al. 2007; Weiß

et al. 2009; Cooray et al. 2010; Scott et al. 2010; Hickox et al. 2012). Alternatively, the clustering peak could be off-centre from the *WISE* source and not on the SCUBA-2 1.5-arcmin map scale. This agrees with Smail et al. (2014) where overdensities of the most active, ultraluminous star-forming galaxies were offset from the assumed protocluster centre and are situated in the lower density environments. Dannerbauer et al. (2014) observed a density of SMGs up to four times greater than in blank-field surveys that were not centred on the submm-bright radio galaxy.

Muldrew, Hatch & Cooke (2015) explored the structures of protoclusters and their relationship with high-redshift galaxies using the Millennium Simulation. They found that protocluster structures are very extended at the redshifts ($z=2$) we are probing with 90 per cent of their mass is dispersed across ~ 30 arcmin ($\sim 35 h^{-1}$ Mpc comoving). This would imply that many observations of protoclusters and high-redshift clusters are not imaging all of the cluster. Many protoclusters have no central or main halo that could be classified as a high-redshift cluster, only 10 per cent were dominated by a single halo at redshift $z=2$. This could explain why there is no evidence or only an upper limit of angular clustering in the Hot DOG and *WISE*/radio AGN fields on ~ 1.5 -arcmin scales from Monte Carlo simulations of typical separations. Alternatively, the cluster might be peaked substantially off-centre from the *WISE* target. Further observations of companion sources in the fields around *WISE*/radio AGNs are needed to determine the angular two-point correlation function $\omega(\theta)$. Wide-field sub(mm) surveys are needed to cover the total (proto)cluster structure, and is in agreement with results from Casey (2016) and Hung et al. (2016), where Casey (2016) found protoclusters subtend 10 arcsec to a half degree in the sky and at redshifts $z \geq 2$ their overdensity is difficult to detect due to their large occupied volumes. Hung et al. (2016) found large-scale structure around a cluster to within 10 arcsec.

Viero et al. (2013) presented observations from *Herschel* and found a clustering signature from SMGs that could be decomposed into two-halo (linear) power from galaxies in separate haloes, and one-halo (non-linear) power from multiple central and satellite galaxies occupying massive haloes. It has been found that a fraction of luminous sources are found within these satellite haloes, for example, González et al. (2011) predict that 38 per cent SMGs and 24 per cent SMGs with $S_{850 \mu\text{m}} > 5$ mJy are satellites. Additionally, star-forming galaxies in groups and clusters were found in the outskirts of massive cluster-scale haloes (Muldrew et al. 2015). The lack of clustering signal of SMGs in the Hot DOG and *WISE*/radio AGN fields could be because they are also in the outskirts of diffuse massive halo and not having enough sources.

5.2 Companion source properties

Only a fraction of the SCUBA-2 companion sources are detected in *WISE*. The *WISE* colours of the companion sources are consistent with star-forming galaxies and AGNs, while their mid-IR to submm ratios are not consistent with AGN-dominated sources (Jones et al. 2015). The companion sources hence appear to be consistent with SMGs. The SMG SFRs were estimated using their submm flux densities and are consistent with SMGs; the average SFR is $\sim 1240 M_{\odot} \text{yr}^{-1}$ for SMGs around *WISE*/radio AGNs, slightly lower than the SFR $\sim 1460 M_{\odot} \text{yr}^{-1}$ for SMGs around Hot DOGs. The SMGs around *WISE*/radio AGNs have slightly higher SFRs than around Hot DOGs by ~ 18 per cent, which is expected that SFRs are enhanced in denser regions.

When comparing the companion SMG sources radio properties to previous SMGs, around 65–70 per cent of bright SMGs

($S_{850 \mu\text{m}} > 7$ mJy) have been detected at $S_{1.4 \text{GHz}}$ (Ivison et al. 2002; Borys et al. 2004). It has been suggested that the radio-undetected SMGs may have colder dust or lie at $z > 3$ (Ivison et al. 2002; Eales et al. 2003; Swinbank et al. 2008). No companion sources have radio detections in shallow NVSS or FIRST images, and the radio data are not deep enough to assess their dust temperatures.

The SFRDs of the *WISE*-selected AGNs are higher than the field but consistent with measurements of clusters of dusty galaxies from HerMES and DSFGs or luminous AGNs. Conclusions from observations of $z > 2$ protoclusters suggest that the Universe's largest galaxy clusters are thought to be built by massive $> 10^{11} M_{\odot}$ galaxies in short-lived bursts of activity. The challenge has been to observe these structures when they have such large volumes, subtending ~ 0.5 deg on the sky (Casey 2016). However, the *WISE*-selected AGNs have high SFRDs with consistent values to these previous observations of clusters of DSFGs, but are on smaller volumes, with a SCUBA-2 map radius of 1.5 arcmin. Therefore, *WISE*-selected AGNs could be used to study protoclusters at high redshift on small volumes (arcmin scales) of the sky.

6 SUMMARY

Previously Hot DOGs and *WISE*-selected AGNs were found to be extremely obscured, hyperluminous AGNs at redshifts between $0.4 < z < 4.6$. Their environments were found to be overdense in SMGs and these overdensities have been investigated here.

- (i) The space densities of SMGs around the *WISE*-selected AGNs were found to be overdense compared to normal star-forming galaxies and SMGs in the S2CLS.
- (ii) The SMGs around *WISE*/radio AGNs have ~ 18 per cent higher SFRs than SMGs around Hot DOGs.
- (iii) The SFRDs of the *WISE*-selected AGNs are higher than field galaxies, and consistent with values for known clusters of dusty galaxies.
- (iv) The results impose an upper limit to the strength of angular clustering of the companion SMG sources in Hot DOGs and *WISE*/radio AGNs on SCUBA-2 1.5-arcmin scales. The typical separations when compared to Monte Carlo simulations showed no angular clustering. This is in agreement with the cumulative fraction of companion sources in different radii from the *WISE* target. This could be because they are satellite galaxies in the massive halo or that the protocluster is on bigger scales (up to ~ 30 arcmin) and we are not fully probing the protocluster.
- (v) Hot DOGs and *WISE*/radio AGNs appear to be signposts of overdense environments.

ACKNOWLEDGEMENTS

The authors thank the anonymous referee for his/her comments and suggestions, which have greatly improved this paper. SFJ thanks Kirsten K. Knudsen for inspiring comments and helpful advice.

This publication makes use of data products from the *Wide-field Infrared Survey Explorer*, which is a joint project of the University of California, Los Angeles and the Jet Propulsion Laboratory/California Institute of Technology, funded by the National Aeronautics and Space Administration. The James Clerk Maxwell Telescope has historically been operated by the Joint Astronomy Centre on behalf of the Science and Technology Facilities Council of the United Kingdom, the National Research Council of Canada and the Netherlands Organisation for Scientific Research. Additional funds for the construction of SCUBA-2 were provided by the

Canada Foundation for Innovation. The program IDs under which the data were obtained were M12AU10, M12BU07 and M13BU02. RJA was supported by FONDECYT grant number 1151408. This work is based in part on observations made with the *Spitzer Space Telescope*, which is operated by the Jet Propulsion Laboratory, California Institute of Technology under a contract with NASA.

REFERENCES

- Adelberger K. L., Steidel C. C., Pettini M., Shapley A. E., Reddy N. A., Erb D. K., 2005, *ApJ*, 619, 697
- Alexander D. M., Smail I., Bauer F. E., Chapman S. C., Blain A. W., Brandt W. N., Ivison R. J., 2005, *Nature*, 434, 738
- Alexander D. M. et al., 2016, *MNRAS*, 461, 2944
- Assef R. J. et al., 2015, *ApJ*, 804, 27
- Barger A. J. et al., 2014, *ApJ*, 784, 9
- Becker R. H., White R. L., Helfand D. J., 1995, *ApJ*, 450, 559
- Blain A. W., Smail I., Ivison R. J., Kneib J.-P., Frayer D. T., 2002, *Phys. Rep.*, 369, 111
- Blain A. W., Chapman S. C., Smail I., Ivison R., 2004, *ApJ*, 611, 725
- Borys C., Scott D., Chapman S., Halpern M., Nandra K., Pope A., 2004, *MNRAS*, 355, 485
- Bouwens R. J. et al., 2011, *ApJ*, 737, 90
- Bridge C. R. et al., 2013, *ApJ*, 769, 91
- Casey C. M., 2016, *ApJ*, 824, 36
- Casey C. M. et al., 2012, *ApJ*, 761, 140
- Casey C. M. et al., 2013, *MNRAS*, 436, 1919
- Casey C. M. et al., 2014, *ApJ*, 796, 95
- Chapman S. C., Blain A. W., Smail I., Ivison R. J., 2005, *ApJ*, 622, 772
- Chapman S. C., Blain A., Ibata R., Ivison R. J., Smail I., Morrison G., 2009, *ApJ*, 691, 560
- Clements D. L. et al., 2014, *MNRAS*, 439, 1193
- Condon J. J., Cotton W. D., Greisen E. W., Yin Q. F., Perley R. A., Taylor G. B., Broderick J. J., 1998, *AJ*, 115, 1693
- Connolly A. J., Szalay A. S., Brunner R. J., 1998, *ApJ*, 499, L125
- Cooper M. C. et al., 2007, *MNRAS*, 376, 1445
- Cooray A. et al., 2010, *A&A*, 518, L22
- Coppin K., Halpern M., Scott D., Borys C., Chapman S., 2005, *MNRAS*, 357, 1022
- Coppin K. et al., 2006, *MNRAS*, 372, 1621
- Croom S. M. et al., 2005, *MNRAS*, 356, 415
- Cowley W. I., Lacey C. G., Baugh C. M., Cole S., 2015, *MNRAS*, 446, 1784
- Dannerbauer H. et al., 2014, *A&A*, 570, A55
- Dempsey J. T. et al., 2013, *MNRAS*, 430, 2534
- DiPompeo M. A., Myers A. D., Hickox R. C., Geach J. E., Hainline K. N., 2014, *MNRAS*, 442, 3443
- Donoso E., Yan L., Stern D., Assef R. J., 2014, *ApJ*, 789, 44
- Eales S., Lilly S., Gear W., Dunne L., Bond J. R., Hammer F., Le Fèvre O., Crampton D., 1999, *ApJ*, 515, 518
- Eales S., Bertoldi F., Ivison R., Carilli C., Dunne L., Owen F., 2003, *MNRAS*, 344, 169
- Efstathiou G., Bernstein G., Tyson J. A., Katz N., Guhathakurta P., 1991, *ApJ*, 380, L47
- Eisenhardt P. R. M. et al., 2012, *ApJ*, 755, 173
- Farrah D. et al., 2006, *ApJ*, 641, L17
- Geach J. E. et al., 2017, *MNRAS*, 465, 1789
- Gobat R. et al., 2013, *ApJ*, 776, 9
- González V., Labbé I., Bouwens R. J., Illingworth G., Franx M., Kriek M., 2011, *ApJ*, 735, L34
- Granato G. L., Ragone-Figueroa C., Domínguez-Tenreiro R., Obreja A., Borgani S., De Lucia G., Murante G., 2015, *MNRAS*, 450, 1320
- Greve T. R., Ivison R. J., Bertoldi F., Stevens J. A., Dunlop J. S., Lutz D., Carilli C. L., 2004, *MNRAS*, 354, 779
- Groth E. J., Peebles P. J. E., 1977, *ApJ*, 217, 385
- Hainline L. J., Blain A. W., Smail I., Frayer D. T., Chapman S. C., Ivison R. J., Alexander D. M., 2009, *ApJ*, 699, 1610
- Hatsukade B., Ohta K., Seko A., Yabe K., Akiyama M., 2013, *ApJ*, 769, L27
- Hickox R. C. et al., 2012, *MNRAS*, 421, 284
- Holland W. S. et al., 2013, *MNRAS*, 430, 2513
- Hopkins P. F., Hernquist L., Cox T. J., Di Matteo T., Robertson B., Springel V., 2006, *ApJS*, 163, 1
- Hung C.-L. et al., 2016, *ApJ*, 826, 130
- Ivison R. J., Smail I., Le Borgne J.-F., Blain A. W., Kneib J.-P., Bezecourt J., Kerr T. H., Davies J. K., 1998, *MNRAS*, 298, 583
- Ivison R. J. et al., 2002, *MNRAS*, 337, 1
- Ivison R. J. et al., 2007, *MNRAS*, 380, 199
- Jarrett T. H. et al., 2011, *ApJ*, 735, 112
- Jones S. F. et al., 2014, *MNRAS*, 443, 146
- Jones S. F. et al., 2015, *MNRAS*, 448, 3325
- Laird E. S. et al., 2009, *ApJS*, 180, 102
- Landy S. D., Szalay A. S., 1993, *ApJ*, 412, 64
- Lilly S. J., Eales S. A., Gear W. K. P., Hammer F., Le Fèvre O., Crampton D., Bond J. R., Dunne L., 1999, *ApJ*, 518, 641
- Lonsdale C. J. et al., 2015, *ApJ*, 813, 45
- Magnelli B., Elbaz D., Chary R. R., Dickinson M., Le Borgne D., Frayer D. T., Willmer C. N. A., 2011, *A&A*, 528, A35
- Mendez A. J. et al., 2016, *ApJ*, 821, 55
- Muldrew S. I., Hatch N. A., Cooke E. A., 2015, *MNRAS*, 452, 2528
- Myers A. D., Brunner R. J., Nichol R. C., Richards G. T., Schneider D. P., Bahcall N. A., 2007, *ApJ*, 658, 85
- Peebles P. J. E., 1980, *The Large-Scale Structure of the Universe*. Princeton Univ. Press, Princeton, NJ
- Pope A., Borys C., Scott D., Conselice C., Dickinson M., Mobasher B., 2005, *MNRAS*, 358, 149
- Pope A. et al., 2006, *MNRAS*, 370, 1185
- Porciani C., Magliocchetti M., Norberg P., 2004, *MNRAS*, 355, 1010
- Rosen S. et al., 2015, in Taylor A. R., Rosolowsky E., eds. *ASP Conf. Ser.*, Vol. 495, *Astronomical Data Analysis Software and Systems XXIV*. Astron. Soc. Pac., San Francisco, p. 319
- Scott S. E., Dunlop J. S., Serjeant S., 2006, *MNRAS*, 370, 1057
- Scott K. S. et al., 2010, *MNRAS*, 405, 2260
- Seoville N. Z. et al., 2000, *AJ*, 119, 991
- Smail I., Ivison R. J., Blain A. W., 1997, *ApJ*, 490, L5
- Smail I., Ivison R. J., Owen F. N., Blain A. W., Kneib J.-P., 2000, *ApJ*, 528, 612
- Smail I. et al., 2014, *ApJ*, 782, 19
- Smolčić V. et al., 2012, *A&A*, 548, A4
- Strazzullo V. et al., 2013, *ApJ*, 772, 118
- Swinbank A. M. et al., 2008, *MNRAS*, 391, 420
- Swinbank A. M. et al., 2014, *MNRAS*, 438, 1267
- Tamura Y. et al., 2009, *Nature*, 459, 61
- Tanaka M. et al., 2013, *ApJ*, 772, 113
- Toft S. et al., 2014, *ApJ*, 782, 68
- Tsai C.-W. et al., 2015, *ApJ*, 805, 90
- Umehata H. et al., 2015, *ApJ*, 815, L8
- Viero M. P. et al., 2013, *ApJ*, 772, 77
- Wake D. A. et al., 2008, *MNRAS*, 387, 1045
- Weiß A. et al., 2009, *ApJ*, 707, 1201
- Wilkinson A. et al., 2017, *MNRAS*, 464, 1380
- Williams C. C. et al., 2011, *ApJ*, 733, 92
- Wright E. L. et al., 2010, *AJ*, 140, 1868
- Wu J. et al., 2012, *ApJ*, 756, 96
- Wylezalek D. et al., 2013, *ApJ*, 769, 79
- Wylezalek D. et al., 2014, *ApJ*, 786, 17
- Yajima H., Shlosman I., Romano-Díaz E., Nagamine K., 2015, *MNRAS*, 451, 418

This paper has been typeset from a $\text{\TeX}/\text{\LaTeX}$ file prepared by the author.